

# Co<sub>2</sub>FeAl Heusler thin films grown on Si and MgO substrates: annealing temperature effect

M. Belmeguenai <sup>\*1</sup>, H. Tuzcuoglu<sup>1</sup>, M. S. Gabor<sup>†2</sup>, T. Petrisor  
jr<sup>2</sup>, C. Tuisan<sup>2,3</sup>, F. Zighem<sup>1</sup>, S. M. Chérif<sup>1</sup> and P. Moch<sup>1</sup>

<sup>1</sup> LSPM-CNRS, Université Paris 13, 99 avenue Jean-Baptiste Clément 93430 Villetaneuse, France

<sup>2</sup> Center for Superconductivity, Spintronics and Surface Science, Technical University of Cluj-Napoca,  
Str. Memorandumului No. 28 RO-400114 Cluj-Napoca, Romania and

<sup>3</sup> Institut Jean Lamour, CNRS, Université de Nancy, BP 70239, F- 54506 Vandoeuvre, France

10 nm and 50 nm Co<sub>2</sub>FeAl (CFA) thin films have been deposited on MgO(001) and Si(001) substrates by magnetron sputtering and annealed at different temperatures. X-rays diffraction revealed polycrystalline or epitaxial growth (according to the relation CFA(001)[110]//MgO(001)[100] epitaxial relation), respectively for CFA films grown on a Si and on a MgO substrate. For these later, the chemical order varies from the *A2* phase to the *B2* phase when increasing the annealing temperature ( $T_a$ ) while only the *A2* disorder type has been observed for CFA grown on Si. Microstrip ferromagnetic resonance (MS-FMR) measurements revealed that the in-plane anisotropy results from the superposition of a uniaxial and of a fourfold symmetry term for CFA grown on MgO substrates. This fourfold anisotropy, which disappears completely for samples grown on Si, is in accord with the crystal structure of the samples. The fourfold anisotropy field decreases when increasing  $T_a$  while the uniaxial anisotropy field is nearly unaffected by  $T_a$  within the investigated range. The MS-FMR data also allow for concluding that the gyromagnetic factor remains constant and that the exchange stiffness constant increases with  $T_a$ . Finally, the FMR linewidth decreases when increasing  $T_a$ , due to the enhancement of the chemical order. We derive a very low intrinsic damping parameter ( $1.1 \times 10^{-3}$  and  $1.3 \times 10^{-3}$  for films of 50 nm thickness annealed at 615°C grown on MgO and on Si, respectively).

PACS numbers:

Keywords: Voltage induced anisotropy, magnetoelastic anisotropy, ferromagnetic resonance, digital correlation image

## I. INTRODUCTION

The future spintronic devices require an ideal spin-polarized electron source, achievable by using a half-metallic Heusler alloys [1, 2], having the composition  $X_2YZ$  ( $X$  being a transition metal element,  $Y$  being another transition metal element and  $Z$  being a group III, IV, or V element). These materials are expected to provide very large magneto-resistive effects when used as magnetic electrodes in magnetic tunnel junctions (MTJs) and in current-perpendicular-to-plane (CPP) spin valves. They can be used as perfect spin filters and spin-injection devices as alternative materials to ferromagnetic 3d metals. Therefore, Co-based Heusler alloys, such as Co<sub>2</sub>FeAl, have attracted much research interest due to their large magnetic moment and their high Curie temperature. Co<sub>2</sub>FeAl (CFA) has a very high Curie temperature (1000 K) and is theoretically predicted to have a half-metallic character arising from its spin-split band structure. It can provide giant tunnelling magneto-resistance (360% at room temperature) [3, 4] when used as an electrode in magnetic tunnel junctions, which makes CFA promising for practical applications. However in such alloys, there is

always some degree of chemical disorder, which strongly influences many of their physical properties. In reality, the totally ordered phase (*L21*) is difficult to achieve and there is a variety of derived structural types arising from atomic disorder in the occupation of the available sites. When the  $X$  atoms occupy their assigned sites for the *L21* phase, while the  $Y$  and  $Z$  atoms randomly share the other ones, the *B2* structure is obtained. The structure *A2* corresponds to a completely random occupation, by any  $X$ ,  $Y$  or  $Z$  atom, of all the existing sites of the *L21* phase. It is reported by Picozzi that some types of disorder might lead to additional states at the Fermi level, thus reducing the spin polarization [5]. In addition to the atomic order, the crystallographic orientation of the Heusler thin film is important and may break the half metallicity. Therefore, an annealing process is required to initiate the crystallization and to induce the atomic ordering. It is thus of great interest to investigate the annealing temperature ( $T_a$ ) effects on the structural and magnetic properties of CFA thin films. The purpose of this paper is to use ferromagnetic resonance in microstrip line (MS-FMR) under an in-plane and a out-of-plane applied magnetic field, combined to vibrating sample magnetometry (VSM), in view of investigating the correlation between structural and magnetic properties of CFA thin films grown on Si or on MgO substrates and annealed at different temperatures. A special attention will be given to the effect of  $T_a$  on the FMR linewidth and damping constant.

\*belmeguenai.mohamed@univ-paris13.fr

†mihai.gabor@phys.utcluj.ro

## II. SAMPLE AND EXPERIMENTAL SET UP

CFA films were grown on MgO(001) and thermally oxidized Si(001)/SiO<sub>2</sub> substrates using a magnetron sputtering system with a base pressure lower than  $3 \times 10^{-9}$  Torr. Prior to the deposition of the CFA films, a 4 nm thick MgO buffer layer was grown at room temperature (RT) by RF sputtering from a MgO polycrystalline target under an Argon pressure of 15 mTorr. Next, 10 nm and 50 nm thick CFA films, were deposited at room temperature by DC sputtering under an Argon pressure of 1 mTorr, at a rate of 0.1 nm/s. Finally, the CFA films were capped with a MgO(4 nm)/Ta(4 nm) bilayer. After the growth of the stack, the structures were ex-situ annealed at different temperatures ( $T_a = 315^\circ\text{C}$ ,  $415^\circ\text{C}$ ,  $515^\circ\text{C}$  and  $615^\circ\text{C}$ ) during 15 minutes in vacuum. The structural properties of the samples have been characterized by X-ray diffraction (XRD) using a four-circle diffractometer. Their magnetic static and dynamic properties have been studied by vibrating sample magnetometer (VSM) and microstrip ferromagnetic resonance (MS-FMR) [6], respectively.

### A. Structural properties

XRD is a standard method for the characterization of the crystal growth properties of thin films. Figure 1 shows the XRD  $\theta - 2\theta$  patterns for 50 nm thick CFA films grown on MgO substrates, annealed at different temperatures and on Si substrates (grazing incidence (GI) configuration) annealed at  $615^\circ\text{C}$ , respectively. The XRD patterns show that, in addition to the (002) peak of the MgO substrate, the CFA films (Fig. 1a) exhibit only two peaks which are attributed to the (002) and (004) diffraction lines of CFA. The (004) peak is expected for the A2 type structure, while the existence of an additional (002) peak indicates a B2 type structure. Since the ratio  $I_{002}/I_{004}$  of the integrated intensities of the (002) and of the (004) peaks increases versus  $T_a$  (Fig. 1c), the chemical order varies from the B2 phase towards the A2 phase when decreasing  $T_a$  [7]. However, the  $I_{002}/I_{004}$  ratio is the significantly below the theoretical expected one for a fully B2 ordered crystal [8]. This seems to indicate that, even after annealing the films at  $615^\circ\text{C}$ , regions with different type of chemical order still coexist. Moreover, using the well known Scherrer equation we determined a mean crystallite size of around 10 nm for MgO grown films irrespective of annealing temperature. This indicates that with annealing temperature we do not have a grain growth of B2 but a crystallization of regions with structural disorder and an improvement of the chemical ordering towards the B2 phase, since both the intensities of (002) and (004) peaks increase with annealing. In contrast, the GIXRD pattern of CFA films grown on Si (Fig. 1b) clearly shows peaks corresponding to CFA (022), (004) and (224) reflections, due to the lack of epitaxial growth in the case of a Si substrate, which gives rise to a polycrystalline

structure. The diffraction patterns exhibit peaks ( $hkl$ ) corresponding only to the  $h + k + l = 4n$  (where  $n$  is an integer) type reflections which seems to indicate that the films show A2 structure with a disorder among Co, Fe, and Al sites. However, a precise evaluation of the chemical order is difficult to perform, due to the relative low diffracted signal. Furthermore, pole figures (not shown here) revealed that CFA grown on Si does not display any in-plane preferential growth direction. In the case of the CFA films grown on MgO,  $\phi$ -scan measurements (see inset of Figure 1a) allow for asserting an epitaxial growth of the CFA films grown on MgO, within the investigated temperature range for Ta, according to the expected CFA(001)[110]//MgO(001)[100] epitaxial relation. Figure 1c shows the variations of the lattice constant for increasing annealing temperatures for different samples. The dashed lines represent the L21 ordered CFA bulk value [9]. For the films deposited on thermally oxidized Si(001)/SiO<sub>2</sub> substrates the lattice constant was obtained by applying the Bragg equation to the corresponding (022) peak. The lattice parameter is larger than the reference value in the as prepared state and decreases with increasing the annealing temperature for CFA for both substrates. The out-of-plane and the in-plane lattice parameters of the CFA films grown on MgO were evaluated using symmetric and asymmetric XRD scans of (004) and (022) type reflections, respectively. From Fig. 1d one can observe that the as-deposited film experiences a relatively strong tetragonal distortion. As the annealing temperature increases the distortion relaxes. In the case of the films annealed at temperatures higher than  $515^\circ\text{C}$  the value of out-of-plane is essentially equal with the value of the in-plane lattice parameters. This type of lattice parameter evolution was previously noticed in CFA/MgO(001) samples [7] and was attributed the residual strain associated with the growth method. Moreover, the lattice parameters of CFA films of identical thicknesses (50 nm), grown on Si or on MgO substrates are very close from each other in the investigated  $T_a$  range, suggesting that the decrease of the lattice parameter is not due to the chemical disorder, but most likely to relaxation of residual strain.

### B. Magnetic properties

All the measurements presented here have been made at room temperature and analyzed using a model based on the following density of energy, which was previously found to be appropriate to describe the properties of Heusler films [10]:

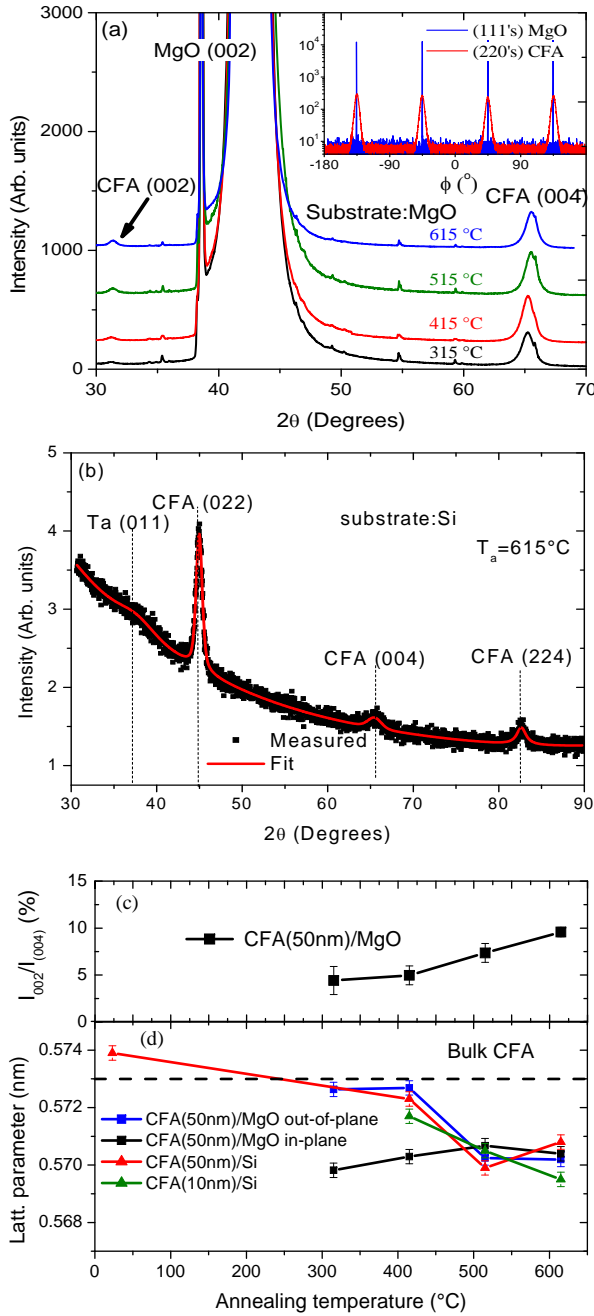


Figure 1: (Colour online) (a) X-ray  $\theta - 2\theta$  diffraction pattern for the 50 nm CFA thick films grown on a MgO substrate annealed at different temperature. The inset represents the  $\phi$ -scans of the substrate and the CFA films annealed at 615°C. (b) X-ray diffraction pattern measured in grazing incidence geometry for the 50 nm CFA thick film grown on a Si substrate annealed at 615°C. The symbols represent experimental data while the lines are the result of the theoretical fit. The vertical dashed lines mark the positions of the Ta(011) and CFA((022), (004), (224)) reflections. (c) Evolution of the ratio of the integral intensities of the (002) and (004) Co<sub>2</sub>FeAl peaks  $I_{(002)}/I_{(004)}$  with respect to the annealing temperatures of 50 nm thick Co<sub>2</sub>FeAl films grown on MgO Substrates. (d) Evolution of the lattice parameter, deduced from the position of the (022) and of the (002) peaks, as function of the annealing temperature in 10 nm and 50 nm thick Co<sub>2</sub>FeAl films grown on Si and CFA substrates.

$$E = -M_S H (\cos(\varphi_M - \varphi_H) \sin \theta_M \sin \theta_H + \cos \theta_M \cos \theta_H) - \frac{1}{2} (1 + \cos(2(\varphi_M - \varphi_u))) K_u \sin^2 \theta_M - (2\pi M_S^2 - K_{\perp}) \sin^2 \theta_M - \frac{1}{8} (3 + \cos 4(\varphi_M - \varphi_4)) K_4 \sin^4 \theta_M \quad (1)$$

In the above expression,  $\theta_M$  and  $\varphi_M$  respectively represent the out-of-plane and the in-plane (referring to the substrate edges) angles defining the direction of the magnetization  $M_S$ .  $\varphi_u$  and  $\varphi_4$  define the angles between an easy uniaxial planar axis or an easy planar fourfold axis, respectively, with respect to this substrate edge.  $K_u$ ,  $K_4$  and  $K_{\perp}$  are in-plane uniaxial, fourfold and out-of-plane uniaxial anisotropy constants, respectively. We define  $H_u = 2K_u/M_S$  and  $H_4 = 4K_4/M_S$  as the in-plane uniaxial and the fourfold anisotropy fields respectively and we introduce the effective magnetization  $M_{eff} = H_{eff}/4\pi$  obtained by:

$$4\pi M_{eff} = H_{eff} = 4\pi M_S - \frac{2K_{\perp}}{M_S} = 4\pi M_S - H_{\perp}$$

The resonance expressions for the frequency of the uniform precession mode and for the perpendicular standing spin waves (PSSW) modes assuming in-plane or perpendicular applied magnetic fields are given in [6]. The experimental results concerning the measured peak-to-peak FMR linewidths  $\Delta H^{PP}$  are analyzed in this work taking account of both intrinsic and extrinsic mechanisms. As discussed in [6], the observed magnetic field linewidth ( $\Delta H^{PP}$ ) is analyzed by considering Gilbert ( $\Delta H^{Gi}$ ) [11], inhomogeneities ( $\Delta H^{inh}$ ) and two magnon scattering ( $\Delta H^{2mag}$ ) [12] contributions. This latter is given by [6]:

$$\Delta H^{2mag} = \Gamma_0 + \Gamma_2 \cos 2(\varphi_H - \varphi_2) + \Gamma_4 \cos 4(\varphi_H - \varphi_4) \arcsin \left( \frac{f}{\sqrt{f^2 + f_0^2 + f_0}} \right) \quad (2)$$

with:  $f_0 = \gamma M_{eff}$ . The expected fourfold symmetry induces the  $\Gamma_0$  and  $\Gamma_4$  coefficients; the coefficient  $\Gamma_2$  is phenomenologically introduced. The total FMR linewidth in our samples can be written as:

$$\Delta H^{PP} = \Delta H^{Gi} + (\Delta H^{mos} + \Delta H^{inh} + \Delta H^{2mag}) \quad (3)$$

The analysis of the variation of the resonance linewidth  $\Delta H^{PP}$  versus the frequency and the in-plane field orientation allows for evaluating  $\alpha$ ,  $\Delta\varphi_H$ ,  $\Delta H^{inh}$ ,  $\Gamma_0$ ,  $\Gamma_2$  (and  $\varphi_2$ ) and  $\Gamma_4$  (and  $\varphi_4$  which, from symmetry considerations, is expected to have a 0° or 45° value, depending upon the chosen sign of  $\Gamma_4$ ).

### 1. Static properties

The easy axis VSM hysteresis loops were measured at different field orientation and the magnetization at saturation has been extracted. The magnetization at saturation of the three samples (not shown here) increases slightly (10% of change) with increasing  $T_a$ , which indicates an improved atomic ordering. A maximum value of 1029 emu/cm<sup>3</sup> can be achieved for a 50 nm CFA thick film grown on a MgO substrate and annealed at 615°C. This value is higher, when compared to a similar CFA film grown on a Si substrate, most probably due to the higher crystalline quality and higher order degree. Figure 2 shows typical hysteresis loops, along the easy axis, as function of the annealing temperature for the 50 nm thick CFA films grown on Si and on MgO substrates. For both substrates a clearly different behaviour is observed between the samples annealed at low and at higher temperature. The increase of the coercive field ( $H_C$ ) with decreasing  $T_a$  is an indication of the improving of the crystalline structure and of the chemical order in the annealed samples. One should mention that the angular dependence of  $M_r/M_S$  (not shown here) of annealed CFA films grown on Si showed a uniaxial anisotropy behaviour. As the annealing temperature increases the sample quality and the chemical order are enhanced and a unique uniaxial anisotropy is observed. This is confirmed by the variation of the uniaxial anisotropy easy axis direction with  $T_a$  as shown below. For the 50 nm thick film grown on a MgO substrate, the measured hysteresis loops revealed a fourfold in-plane magnetic anisotropy with (110) easy and (100) hard axis directions to which a weak uniaxial magnetic anisotropy is superimposed. The intermixing of various chemical ordered phases or even possible amorphous regions of CFA grown on MgO substrate, as revealed by XRD, generates regions within the film with different magnetocrystalline anisotropy. Therefore the measured hysteresis loops results in poor squariness which gets improved as the annealing temperature increases due to the enhancement of the disorder. Full square easy axis hysteresis loop has been obtained for CFA thin films annealed at 750°C (not shown here).

### 2. Dynamic properties

The uniform precession and the first perpendicular standing spin wave (PSSW) modes have been observed in perpendicular and in-plane applied field configurations for the 50 nm thick films while for the 10 nm thick film, no PSSW mode is detected due to their high frequency over-passing the available bandwidth (0-24 GHz). Typical perpendicular field dependences of the resonance frequencies of the uniform and of the PSSW modes are shown on figure 3 for the CFA film grown on Si. By fitting the data in figure 3 to the model presented above, the gyromagnetic factor ( $\gamma$ ), the exchange stiffness constant ( $A_{ex}$ ) and the effective magnetization ( $4\pi M_{eff}$ ) are

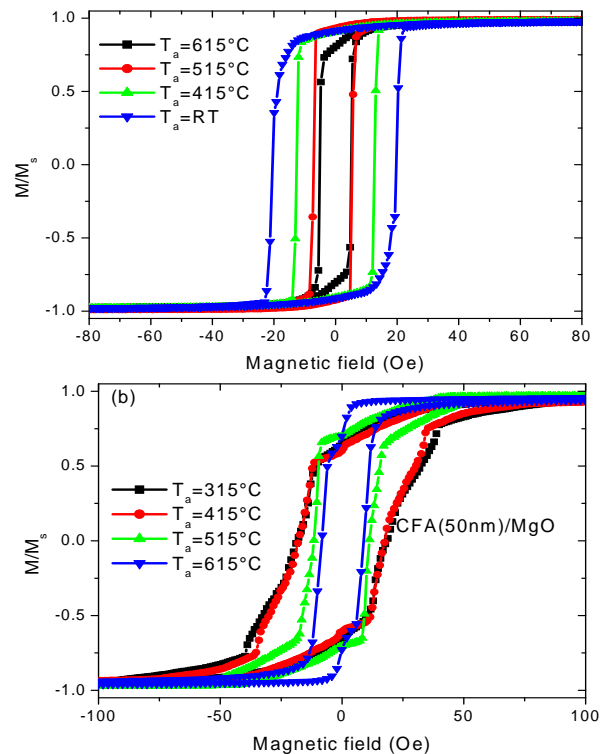


Figure 2: (Colour on line) Hysteresis loops, along the easy axis, of the 50 nm thick CFA films annealed at different temperatures and grown on (a) a Si substrate (b) a MgO Substrate.

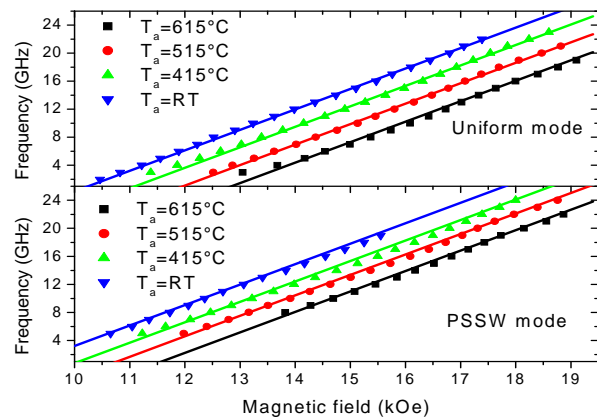


Figure 3: (Colour on line) Variation of the frequencies of the uniform and of the PSSW modes for 50 nm thick CFA films annealed at different temperatures. Solid lines indicate the fit using the model described in the text.

extracted. The fitted  $\gamma/2\pi = 29.2$  GHz/T is independent on  $T_a$  while  $A_{ex}$  (Fig. 4b) decreases versus  $T_a$ , suggesting an enhancement of the chemical order when the annealing temperature increases, presumably due to the enhancement of the chemical order. A similar behaviour of the exchange stiffness of  $\text{Co}_2\text{FeAl}_{0.5}\text{Si}_{0.5}$  [13] with  $T_a$  has

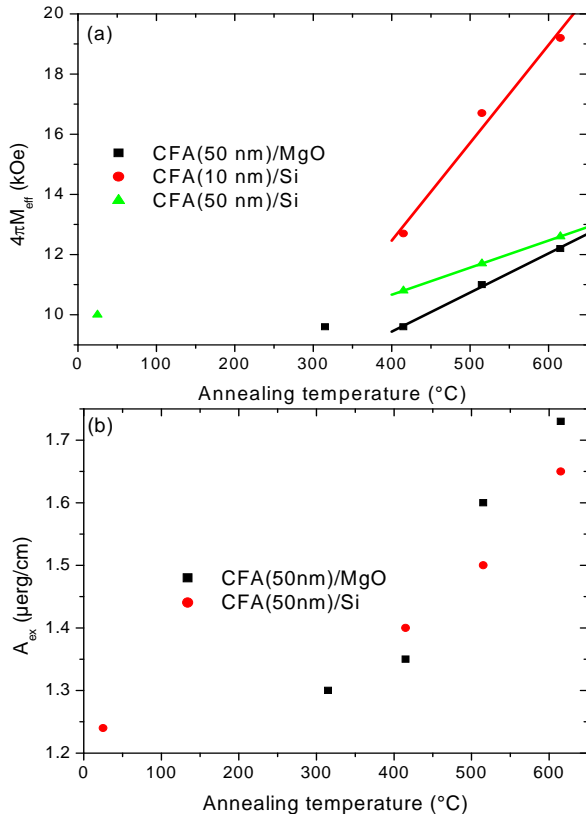


Figure 4: (Colour on line) Variations of (a) the effective magnetization ( $4\pi M_{eff}$ ) and of the (b) exchange stiffness constant ( $A_{ex}$ ), as function of the annealing temperature, of 10 nm and 50 nm thick CFA films grown on Si and on MgO substrates. The solid lines refer to the linear fit in the range 400-650°C.

been reported by Trudel *et al.* The smaller  $A_{ex}$  values of CFA films grown on Si compared to those grown on MgO is another indication of the best crystalline structure and chemical order of these latter.

Interestingly, the extracted effective magnetization from the MS-FMR measurements, shown on figure 4a increases linearly with the annealing temperature leading to negative perpendicular anisotropy, which tends to favour the in-plane orientation. This effect is more pronounced for the 10 nm thick film: the slope of this linear dependence, in the range 415°C-615°C, decreases from 32 Oe/°C to 9 Oe/°C respectively for the 10 nm and for the 50 nm thick CFA films grown on Si. The 50 nm CFA thick film shows a larger slope (13 Oe/°C) compared to the similar CFA film grown on Si. This effect originates from the interface CFA/MgO, which is improved through the increasing of the annealing temperature. Moreover, a linear variation of  $4\pi M_{eff}$  as function of the thickness inverse of CFA films, annealed at  $T_a = 600^\circ\text{C}$  and deposited on MgO [6] and on Si substrates, has been observed. This thickness dependent anisotropy was also observed in structures based on CoFeB/MgO [14], but unlike CFA/MgO, the CoFeB/MgO interface favours a perpendicular magnetization. Moreover, it is worth men-

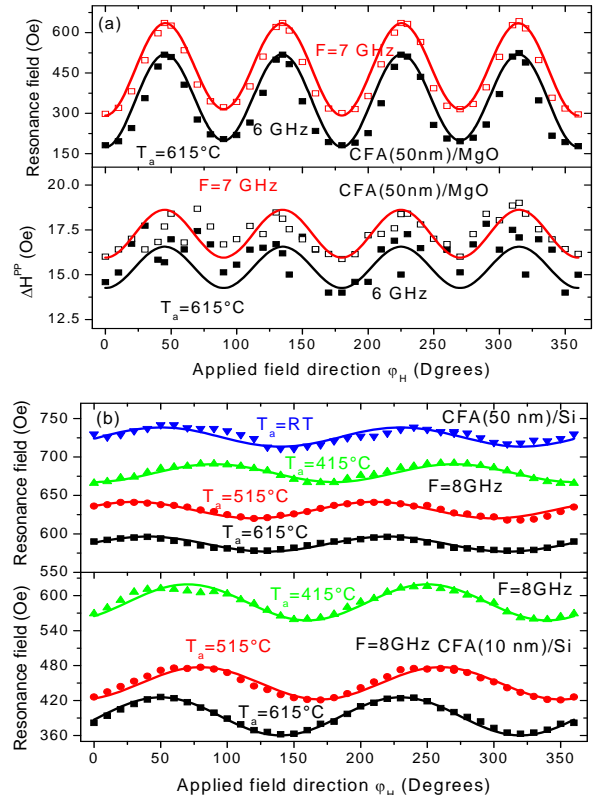


Figure 5: (Colour online) Angular dependence of the resonance field and of the peak to peak field FMR linewidth ( $\Delta H^{PP}$ ) of 10 nm and 50 nm thick CFA thin films grown on (a) MgO and on (b) Si substrates. The solid lines refer to the fit using the model described in the text.

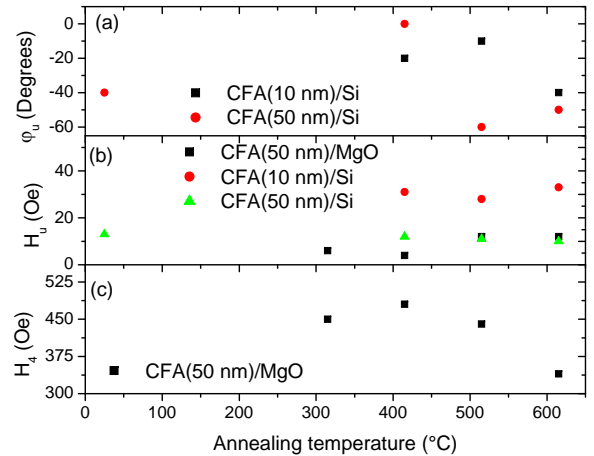


Figure 6: (Colour online) Annealing temperature dependence of the (a) uniaxial anisotropy easy axis direction (b) uniaxial ( $H_u$ ) and of the (c) fourfold anisotropy fields ( $H_4$ ) of the 10 nm and 50 nm CFA thick films grown on Si and MgO substrates.

tioning in the case of Ta/CFA/MgO multilayers the surface anisotropy favours also perpendicular magnetization [15]. Figure 5 shows the typical MS-FMR angular dependence of the resonance field at 7 GHz and 8 GHz driven frequency for three investigated CFA thick films annealed at various  $T_a$ . For the 50 nm CFA thick film grown on MgO, the angular dependence is only presented at  $T_a = 615^\circ\text{C}$  for clarity. The MS-FMR measurements show that the angular behavior of the resonance field is governed by a uniaxial anisotropy or a superposition of uniaxial and fourfold anisotropies, respectively for films grown on Si and on MgO substrates. The disappearance of the fourfold anisotropy for CFA grown on Si is directly correlated to their in-plane polycrystalline structure due to the amorphous  $\text{SiO}_2$  layer. The uniaxial anisotropy field ( $H_u$ ), presented on Figure 6b, is unaffected by  $T_a$  for all the samples. However, in contrast the CFA films grown on MgO, the direction of the uniaxial anisotropy easy axis ( $\varphi_u$ ), determined with a  $90^\circ$  precision since it is referenced with respect to substrate edges, varies with  $T_a$  in the case of CFA thin films grown on Si substrates as shown on Fig. 6a, which complicates the identification of its origin. Therefore, a completely satisfactory interpretation of the presence of  $H_u$  and of its  $T_a$  dependency is still missing. For the 50 nm CFA thick film grown on MgO, the uniaxial and the fourfold anisotropies show parallel easy axes which remain independent of  $T_a$ : this common axis coincides with one of the substrate edges ( $\varphi_u = \varphi_4 = 0$ ) and, consequently, with one of the  $\langle 110 \rangle$  crystallographic directions of the CFA phase. The decrease of the fourfold anisotropy field ( $H_4$ ) as  $T_a$  increases (Fig. 6c) is an effect of the improving crystalline structure and of the enhancement of the chemical order.

The FMR linewidth is a measure of the relaxation rate of the magnetization and is related to the magnetic damping. This linewidth is caused by two mechanisms: the intrinsic damping of the magnetization and extrinsic contributions [16] (such as two magnons scattering, mosaicity, ...). The angular and frequency dependences of the FMR linewidth provide information about these magnetic damping mechanisms. Therefore, the field peak to peak FMR linewidth, defined as the field difference between the extrema of the sweep-field measured FMR spectra, has been investigated as function of the annealing temperature.

In figure 5a, the FMR peak to peak linewidth ( $\Delta H^{PP}$ ) is plotted as a function of the field angle  $\varphi_H$ , using 6 GHz and 7 GHz driving frequencies, for the 50 nm CFA films grown on a MgO substrate and annealed at  $615^\circ\text{C}$ . In the CFA samples grown on MgO, the  $\Delta H^{PP}$  angular variation shows a perfect fourfold symmetry (in agreement with the variation of the resonance position) while it shows a uniaxial behaviour in the case of CFA grown on Si. Such behavior is characteristic of a two magnons scattering contribution. This effect is correlated to the presence of defects preferentially oriented

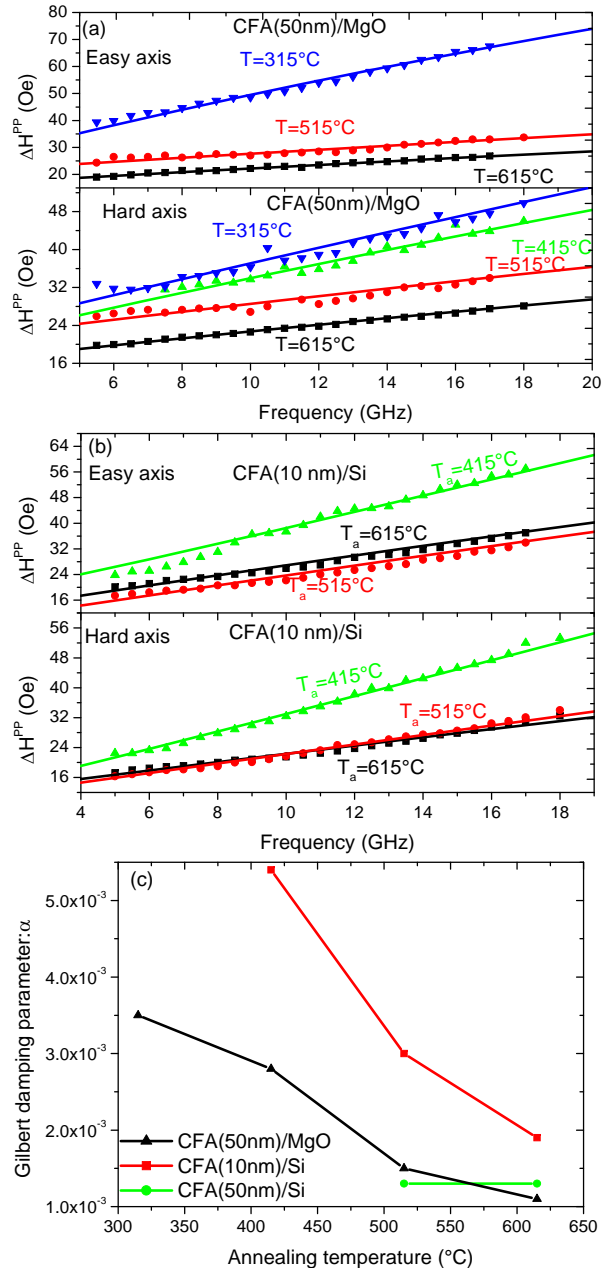


Figure 7: (Colour online) Frequency dependence of the easy and of the hard axes peak to peak field FMR linewidth ( $\Delta H^{PP}$ ) for (a) 50 nm CFA thick films grown on MgO and for (b) 10 nm CFA thick films grown on Si. The solid lines refer to the fit using the model described in the text. (c) Annealing temperature dependence of the Gilbert damping parameter of 10 nm and 50 nm CFA thin films grown on Si and MgO substrates.

along specific crystallographic directions, thus leading to an anisotropic damping. All the other samples show a qualitatively similar behaviour to one of the samples presented here. The positions of the extrema depend on the sample. The observed pronounced anisotropy of the

| $d$ (nm)      | $\Gamma_0$ | $\Gamma_1$ | $\Gamma_2$ | $\varphi_2$ (deg.) | $\varphi_4$ (deg.) | $\Delta H^{inh}$ (Oe) | $\alpha$             | $T_a$ ( $^{\circ}C$ ) |
|---------------|------------|------------|------------|--------------------|--------------------|-----------------------|----------------------|-----------------------|
| MgO substrate |            |            |            |                    |                    |                       |                      |                       |
| 50            | 11         | np         | -1         | np                 | 0                  | 15.2                  | $1.1 \times 10^{-3}$ | 615                   |
| 50            | 8          | np         | -1         | np                 | 0                  | 20                    | $1.5 \times 10^{-3}$ | 515                   |
| 50            | 29         | np         | 17         | np                 | 0                  | 20                    | $3.5 \times 10^{-3}$ | 315                   |
| Si substrate  |            |            |            |                    |                    |                       |                      |                       |
| 10            | 35         | 13         | np         | -40                | np                 | 11                    | $1.9 \times 10^{-3}$ | 615                   |
| 10            | 12         | -8         | np         | -10                | np                 | 8.5                   | $3 \times 10^{-3}$   | 515                   |
| 10            | 31.5       | -7.5       | np         | -20                | np                 | 1                     | $5.4 \times 10^{-3}$ | 315                   |

Table I: Magnetic parameters obtained from the best fits to our experimental FMR results with the above-mentioned model. np: not pertinent.

linewidth cannot be due to the Gilbert damping contribution, which is expected to be isotropic, and must be due to additional extrinsic damping mechanisms.

Figure 7 presents the frequency dependence of FMR linewidth, for an applied field parallel to the easy and the hard axes, of 50 nm and 10 nm thick CFA films annealed at various temperatures and grown respectively on MgO and Si substrates. It shows that the linewidth decreases with increasing  $T_a$  due to the enhancement of the chemical order. The observed angular and frequency dependences of the field linewidth have been analyzed jointly by considering intrinsic (Gilbert), two magnon scattering and inhomogeneities contributions, using the similar method described in [6] and expression (3). Consequently,  $\Gamma_0$ ,  $\Gamma_2, \Gamma_4$ ,  $\varphi_2$ ,  $\varphi_4$  modelling the two magnon contribution, obtained from the best fit of the FMR data are listed in Table I, which also contains the parameters describing the damping effects and of the inhomogeneity. Figure 7c shows the  $T_a$  dependence of the Gilbert damping constant ( $\varphi_4$ ). The CFA films grown on MgO present a smaller damping parameter compared to those grown on Si. The 50 nm thick CFA film, annealed at  $615^{\circ}C$ , shows a very low  $\alpha$ , equal to 0.0011, which is comparable to that of the epitaxial Fe<sub>0.73</sub>V<sub>0.27</sub>, which is considered as the ferromagnetic metal having the lowest  $\alpha$  [17]. However, the 10 nm thick sample shows relatively large values of  $\alpha$  which decrease with increasing  $T_a$ . The reason for both these larger values for thinner films and for the decrease of  $\alpha$  with increasing  $T_a$ , is most probably due to increase of the chemical order degree [18].

### III. CONCLUSION

Co<sub>2</sub>FeAl films with thicknesses of 10 nm and of 50 nm were prepared by sputtering on Si(001)/SiO<sub>2</sub> and

MgO(001) substrates and annealed at various temperatures. They show a polycrystalline structure and an epitaxial growth when Si and MgO substrates are used, respectively. The chemical order changes from *A2* structure to *B2* when increasing the annealing temperature ( $T_a$ ). The microstrip ferromagnetic resonance (MS-FMR) has been used to study the dynamic properties. The MS-FMR has been adjusted to a model allowing for the determination of the most relevant parameters. The in-plane uniaxial anisotropy field, present in all the samples, is unaffected by  $T_a$  and the fourfold anisotropy field, observed in the sample grown on MgO, decreases when increasing the annealing temperature. The presence of this fourfold anisotropy is directly correlated to the crystalline structure of CFA grown on MgO. The effective magnetization increases drastically with  $T_a$ , due to the enhancement of the CFA/MgO interface quality. The angular and frequency dependences of the FMR linewidth, which decreases with increasing annealing temperature, are governed by two magnons scattering and by a Gilbert damping which decreases with the increasing annealing temperature due to the chemical disorder.

### Acknowledgments

This work was partially supported by POS CCE Project ID.574, code SMIS-CSNR 12467 and "SPIN-TAIL" PN-II-ID-PCE-2012-4-0315.

[1] [1] H. C. Kandpal, G. H. Fecher, and C. Felser, J. Phys. D 40, 1507 (2007)  
[2] [2] R. A. de Groot, F. M. Mueller, P. G. van Engen and K. H. J. Buschow, Phys. Rev. Lett. 50, 2024 (1983)

[3] [3] W. H. Wang, H. Sukegawa, and K. Inomata, Phys. Rev. B 82, 092402 (2010)  
[4] [4] W. H. Wang, H. Sukegawa, R. Shan, S. Mitani, and K. Inomata, Appl. Phys. Lett. 95, 182502 (2009).

- [5] [5] S. Picozzi, A. Continenza and A. J. Freeman, Phys. Rev. B 69, 094423 (2004)
- [6] [6] M. Belmeguenai, H. Tuzcuoglu, M. S. Gabor, T. Petrisor Jr. C. Tiusan, D. Berling, F. Zighem, T. Chauveau, S. M. Chérif and P. Moch, Phys. Rev. B, 87, 184431 (2013)
- [7] [7] M. S. Gabor, T. Petrisor Jr., and C. Tiusan, M. Hehn and T. Petrisor, Phys. Rev. B 84, 134413 (2011)
- [8] [8] K. Inomata, N. Ikeda, N. Tezuka, R. Goto, S. Sugimoto, M. Wojcik and E. Jedryka, Sci. Technol. Adv. Mater. 9, 014101, (2008)
- [9] [9] H. J. Elmers, S. Wurmehl, G. H. Fecher, G. Jakob, C. Felser and G. Schönhense, Appl. Phys. A 79, 557 (2004)
- [10] [10] M. Belmeguenai, F. Zighem, Y. Roussigné, S. M. Chérif, P. Moch, K. Westerholt, G. Woltersdorf and G. Bayreuther Phys. Rev. B79, 024419 (2009)
- [11] [11] B. Heinrich and J. F. Cochran, J. Appl. Phys. 57, 3690 (1985).
- [12] [12] A. K. Srivastava, M. J. Hurben, M. A. Wittenauer, P. Kabos, C. E. Patton, R. Ramesh, P. C. Dorsey and D. B. Chrisey, J. Appl. Phys.85, 7838 (2009)
- [13] [13] S. Trudel, G. Wolf, J. Hamrle, B. Hillebrands, P. Klaer, M. Kallmayer, H. J. Elmers, H. Sukegawa, W. Wang, and K. Inomata, Pysc. Rev. B 83, 104412 (2011)
- [14] [14] S. Ikeda, K. Miura, H. Yamamoto, K. Mizunuma, H. D. Gan. M. Endo, S. Kanai, J. Hayakawa, F. Matsukura and H. Ohno, Nature Mater. 9, 721 (2010)
- [15] [15] M. S. Gabor, T. Petrisor Jr., C. Tiusan and T. Petrisor, J. Appl. Phys. 114, 063905 (2013)
- [16] [16] Kh. Zakeri, J. Lindner, I. Barsukov, R. Meckenstock, M. Farle, U. von Hörsten, H. Wende, W. Keune, J. Rucker, S. S. Kalarickal, K. Lenz, W. Kuch and K. Baberschke, Phys. Rev. B 76, 104416 (2007)
- [17] [17] C. Scheck, L. Cheng, I. Barsukov, Z. Frait and W. E. Bailey, Phys. Rev. Lett. 98, 117601 (2007)
- [18] [18] S. Mizukami, D. Watanabe, M. Oogane, Y. Ando, Y. Miura, M. Shirai and T. Miyazaki, J. Appl. Phys.105, 07D306 (2009)